Molecular Therapy
Methods & Clinical Development
Original Article

Ionizable lipid nanoparticles with functionalized PEG-lipids increase retention in the tumor microenvironment

Matthew Jester,[1,3] Rebecca M. Haley,[1,3] Margaret M. Billingsley,[1] Christian Figueroa-Espada,[1] Ryann A. Joseph,[1] Xuexiang Han,[1] and Michael J. Mitchell[1,2]

[1]Department of Bioengineering, University of Pennsylvania, Philadelphia, PA 19104, USA; [2]Penn Institute for RNA Innovation, Perelman School of Medicine, University of Pennsylvania, Philadelphia, PA 19104, USA

This study explores the efficacy of ionizable lipid nanoparticles (LNPs) modified with various functionalized polyethylene glycol (PEG)-lipids for retention within the tumor microenvironment after intratumoral (IT) injection. LNPs were synthesized and characterized with four different functionalized PEG-lipids, and the top performing lipids were evaluated under formulation conditions that varied the ratio of non-modified to functionalized PEG within the LNP. These LNPs were evaluated for size, polydispersity index, zeta potential, pKa, and mRNA encapsulation efficiency, with subsequent *in vitro* analysis of transfection and association efficiency to HepG2 liver cancer cells. Results demonstrated that LNPs formulated with PEG-folate and PEG-maleimide showed increased association to and interaction with cancer cells, compared with the base LNP formulation, which contained only non-functionalized lipid-PEG. *In vivo* studies showed increased retention of surface functionalized LNPs after IT injection in a xenograft model of hepatoblastoma. By slightly modifying LNPs in this manner, it is possible to develop delivery platforms that are better suited for local intratumoral administration. Ultimately, this research underscores the potential of LNPs as a vehicle for localized cancer therapy and emphasizes the need for future investigation into the long-term retention and therapeutic efficacy of LNP formulations.

INTRODUCTION

Solid tumor cancers account for more than 90% of adult human cancers and come with significant treatment challenges.[1] Surgical removal of solid tumors can be an effective first line of defense. However, patients with late-stage cancer diagnoses, metastatic sites, or who are poor candidates for surgical resection are limited in the current treatment landscape to primarily systemically administered therapies such as chemotherapy or immunotherapy.[2] These treatments can have significant clinical impact and are easy to administer,[3] but have numerous challenges for both safety and efficacy. Systemic administration leads to both low accumulation of drug at the tumor site and as well as non-specific binding to other proteins and tissues in the body[3] and is therefore characterized by significant off-target effects that can greatly impact quality of life and severely limit maximum dosage. As an example, it is estimated that less than 0.5% of the total dose of paclitaxel becomes available to the tumor when injected intravenously.[4] Many groups have introduced nanoparticle delivery systems as a method to improve tumor accumulation and targeting after systemic administration, leveraging the enhanced permeability and retention (EPR) effect.[5,6] However, analyses of these types of systems have found EPR not to be as significant as previously believed and that, on average, only 0.7% of the administered nanoparticle dose is delivered to solid tumors.[7,8]

Direct injection of anticancer drugs into the tumor site could alleviate many of these issues, allowing for high local concentration of anti-cancer therapeutics and limited off-site binding and effects.[9] However, although direct injection into the tumor site improves retention and local concentration compared with systemic circulation, the improvement is often marginal and overall retention is still poor, due in part to the anomalous vasculature present in the solid tumor microenvironment (TME).[10,11] Therefore, for direct tumor injections to be clinically feasible, therapeutics must be delivered in a fashion which allows for retention within the TME.

Ionizable lipid nanoparticles (LNPs) are widely known for their role in the Pfizer-BioNTech and Moderna coronavirus disease 2019 vaccines, enabling the efficient delivery of mRNA to human cells.[12–14] LNPs are also used for cancer therapies—including solid tumor cancer therapies[15]—utilizing their nanosc size to permeate the anomalous vasculature of the TME.[16] LNPs offer a versatile platform for encapsulating a wide variety of therapeutic agents, including small molecule drugs, proteins, and nucleic acids,[4,17,18] which can be effective as chemotherapeutics, immunotherapies, or cancer vaccines.[19,20] The modifiable surface of

Received 25 September 2024; accepted 24 March 2025;
https://doi.org/10.1016/j.omtm.2025.101457.

[3]These authors contributed equally

Correspondence: Michael J. Mitchell, PhD, School of Engineering and Applied Science, University of Pennsylvania, Philadelphia, PA 19104, USA.
E-mail: mjmitch@seas.upenn.edu

LNPs can be tailored for both passive and active targeting,[21] including the conjugation of antibodies or ligands to bind to tumor-specific antigens or receptors, respectively.[22]

While ligand- or receptor-specific surface modifications are of interest, a surface modification to universally improve retention of LNPs within the TME would be of great use.[23] Recently, conjugates of lipid-anchored polyethylene glycol (PEG), a constituent in LNP formulations, have come to the attention of researchers as a way to passively target cancer cells.[24,25] PEG has been a highly studied component of the LNP system,[26] and it is well known to play a role in the LNP fate *in vivo*, including influence of the protein corona for improved circulation times and evasion of clearance by the mononuclear phagocyte system.[27,28]

In this study, we evaluate the inclusion of PEG-lipids with a variety of commercially available functional groups—folate, carboxylic acid, PDP, and maleimide—with the ultimate goal of enabling LNP retention in the TME *via* adherence to and interaction with cancer cells. PEG-folate was chosen due to its high affinity to bind to folate receptors, which are commonly overexpressed on various cancer cells.[29–31] PEG-maleimide has been used in our lab previously to conjugate antibodies to the surface of LNPs,[32,33] but unreacted PEG-maleimide LNPs have shown substantially different cellular interactions compared to non-modified LNPs, leading to the conclusion that there is some interaction at play between the maleimide group and the cancer cell, either a reaction with surface thiol groups, or a more generalized change in surface charge or structure post-hydrolysis.[34–39] To further probe the possibility for non-specific cancer cell interactions, PEG-PDP and PEG-carboxylic acid were chosen as additional functional groups that may have specific or generalized cancer cell interactions,[34,35,40,41] as well as integrin adhesion and improved stability.[42,43] These lipids are more commonly used for conjugation chemistry, but are evaluated here without further chemical addition. A previously optimized LNP formulation utilizing the commercially available ionizable lipid C12-200 was used as a base particle throughout this study as a positive control.[32,33,44]

RESULTS

LNP library design and synthesis

Five LNP formulations—four experimental and one base—were synthesized for analysis of association and mRNA delivery to HepG2 liver cancer cells. Microfluidic mixing of an ethanol phase containing lipid components and an aqueous phase containing mRNA was used to formulate LNPs (Figure 1A). The base formulation was a previously optimized LNP formulation of excipients in the following molar ratios: 35% C12-200 ionizable lipid, 46.5% cholesterol, 16% 1,2-dioleoyl-sn-glycero-3-phosphoethanolamine (DOPE), and 2.5% PEG.[44–46] The four experimental formulations included the substitution of part of the 2.5% PEG with PEG-folate (Figure 1B), PEG-carboxylic acid (Figure 1C), PEG-PDP (Figure 1D), or PEG-maleimide (Figure 1E)—all purchased commercially—at a 1:4 M ratio with non-modified PEG.[32,33]

The initial five LNPs were characterized for size, polydispersity index (PDI), zeta potential, encapsulation efficiency, and pKa (Figure 2B). Most functionalized-PEG LNPs caused a slight increase in size, with folate showing a larger increase in size (262 nm) and carboxylic acid showing a decrease in size (62 nm), with the remainder of formulations ranging between 84 and 106 nm, which is typical of mRNA LNPs. Of all LNPs tested, only the maleimide LNP was found to have a statistically similar size to the base formulation (Figure S1A). The zeta potential from the five LNPs ranged from 8 to 17 mV, with the base formulation being in the middle of all formulations tested, at 10 mV, and only the folate LNP being statistically similar to the base (Figure S1B). However, all LNPs could be considered neutrally charged. Encapsulation efficiencies for the five LNPs ranged from 88.5% to 94.4%, showing efficient encapsulation of mRNA regardless of functionalized PEG. Finally, pKa values ranged from 4.63 to 5.75, demonstrating that all LNPs retain an ionizable nature. Additionally, cytotoxicity was measured, and none of the LNP formulations significantly altered cell viability compared to base LNP treated cells (Figure S1C).

In vitro LNP transfection of and association to HepG2 cells

After LNP characterization, LNPs were evaluated for mRNA delivery and association efficiency to HepG2 cells *in vitro*. To evaluate association efficiency, DiO-labled LNPs were exposed to cells ranging from 1 to 60 min (Figure 2C). Fluorescence was measured before and after washes to determine the percentage of LNPs that either adhere to the surface of cells or internalize during that time. Using this method, carboxylic acid, and PDP were identified as modifications that decreased association and cellular interaction, with lower maximum signal at 60 min (Figure 2D). In contrast, folate and maleimide functionalized LNPs perform similarly to the base formulation, with folate functionalized LNPs showing a slight improvement at the 1 min time point, although this was not statistically significant. The purpose of this study was to evaluate the impact of functionalized PEG-lipids in LNP formulation to maximize particle retention in the TME.

To evaluate transfection, LNP-treated cells were measured for mRNA expression using flow cytometry (Figures 2E and S3). Four replicate treatments were performed for each LNP formulation. Unsurprisingly, the base formulation resulted in mRNA delivery and GFP expression in over 80% of cells. Interestingly, all functionalized PEG-lipids reduced cytosolic delivery, measured by mRNA expression. It has been well established that the presence of PEG-lipids can decrease cellular uptake *in vitro*, even as it increases expression *in vivo*.[6] This is due to the PEG shielding effect, which causes a physical barrier between the LNP and cells and proteins. *In vivo*, this is needed to protect from the mononuclear phagocyte system and allow for a viable half-life. However, *in vitro*, this typically causes reduced cellular interaction and can limit particle uptake. For these functionalized PEG-lipids, it was hypothesized that this PEG mechanism would be opposed to the binding mechanisms of the functional groups. However, based on the significant reduction in mRNA expression with higher surface adhesion—especially present in the

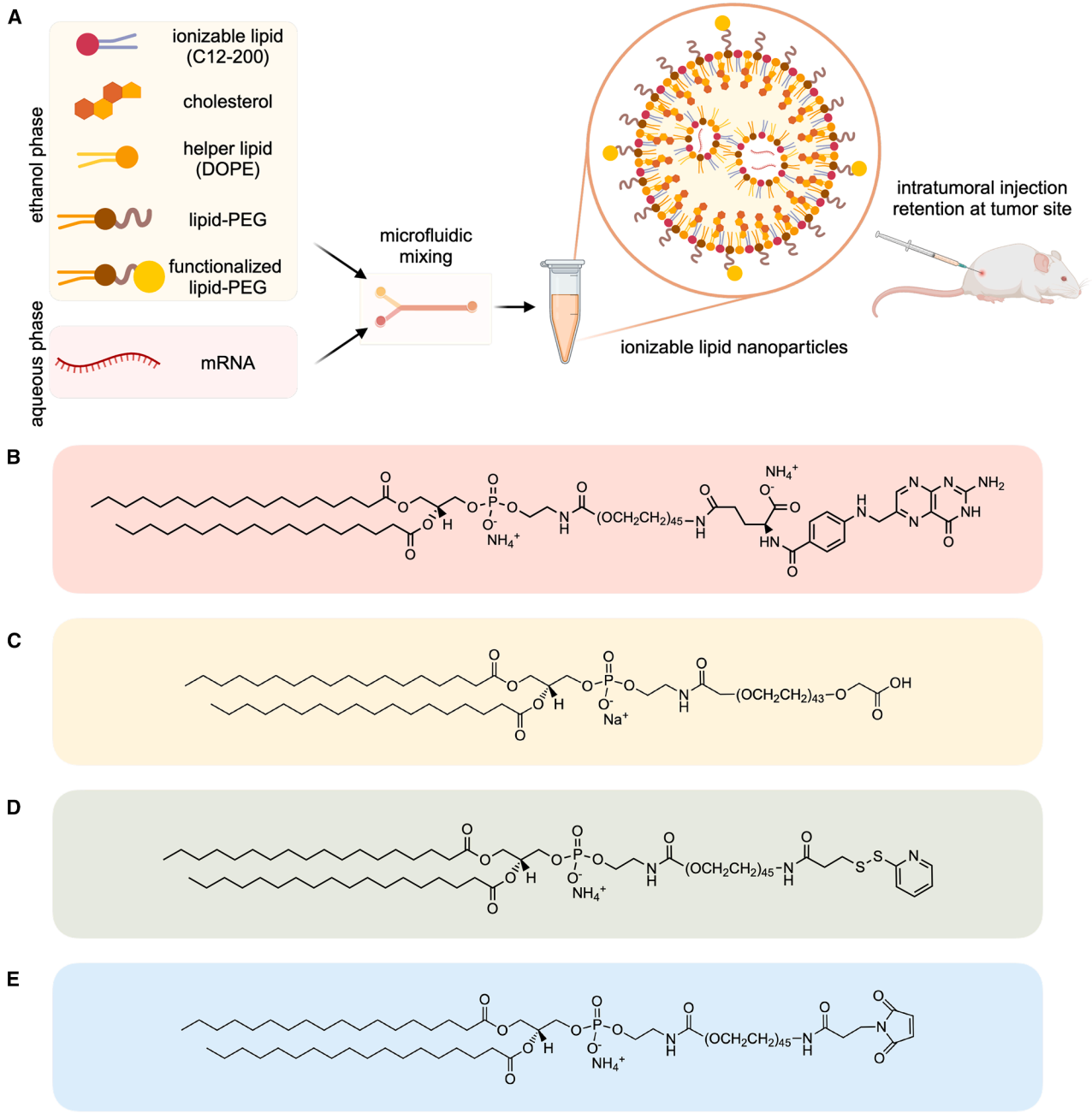

Figure 1. Synthesis of LNPs with functionalized polyethylene glycol-lipids

(A) Schematic of LNP components, formulation, synthesis, expected structure, and application in solid tumor models. An ethanol phase containing an ionizable lipid (C12-200), cholesterol, DOPE, and PEG-lipids is mixed using a microfluidic device with an aqueous phase containing mCherry or GFP mRNA to form LNPs. Structure of (B) DSPE-PEG(2000) folate (PEG-folate), (C) DSPE-PEG(2000) carboxylic acid (PEG-CA), (D) DSPE-PEG(2000) PDP (PEG-PDP), and (E) DSPE-PEG(2000) maleimide (PEG-maleimide) used in experimental LNP formulations.

folate and maleimide modified LNPs—it seems that modifications could amplify this disparity, causing more cell surface interaction but further impeding uptake. The folate- and maleimide-modified LNPs show the greatest effect and were consequently chosen for further *in vitro* and *in vivo* evaluation.

Evaluation of increased percentages of functionalized PEG-lipids

In initial assays, the folate- and maleimide-modified LNPs were synthesized with a 1:4 ratio of functionalized PEG-lipid to non-modified PEG. In this further analysis, additional ratios were

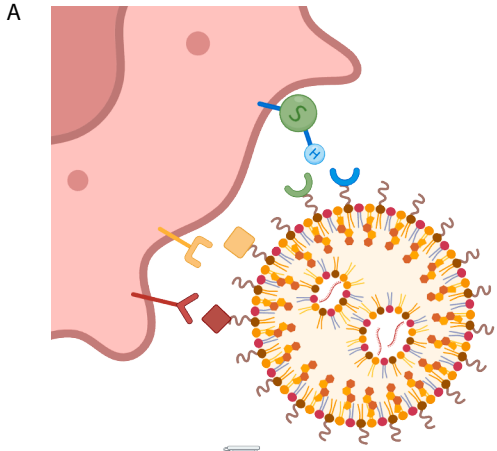

B

LNP Formulation	Z-Average Size (nm) [PDI]	Zeta Potential (mV)	Encapsulation Efficiency (%)	pKa
Base	83.96 ± 1.07 [0.069]	10.31 ± 0.41	94.4 ± 0.9	4.95
Folate (1:4)	262.2 ± 32.78 [0.208]	9.72 ± 0.21	88.5 ± 1.4	4.63
Carboxylic Acid (1:4)	62.2 ± 0.72 [0.066]	8.15 ± 1.95	94.2 ± 2.8	5.75
PDP (1:4)	106.37 ± 2.84 [0.208]	16.93 ± 0.40	92.8 ± 3.1	5.73
Maleimide (1:4)	100.29 ± 11.3 [0.265]	15.07 ± 0.25	90.4 ± 4.8	5.65

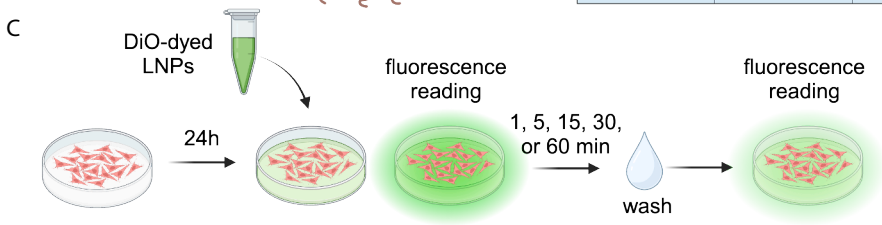

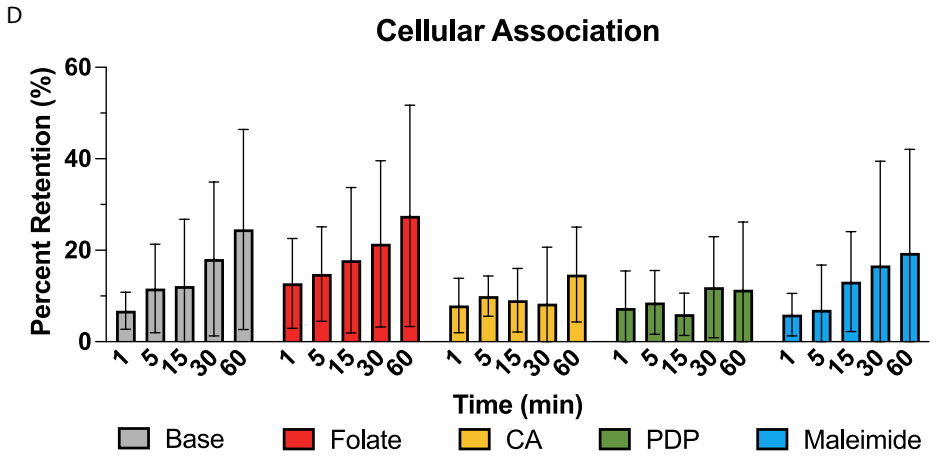

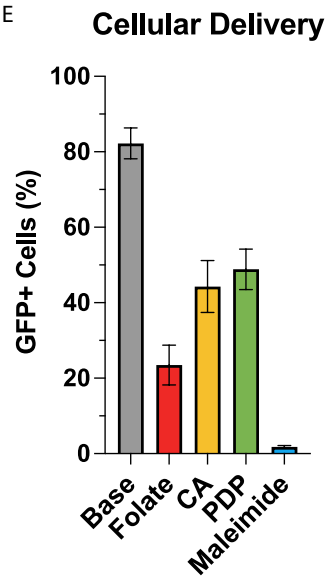

Figure 2. Transfection and association efficiency of LNPs with functionalized PEG-lipids

(A) Schematic demonstrating pathways for functionalized PEG-lipid surface active chemistries. (B) Measurements of z-average, PDI, zeta potential, mRNA encapsulation efficiency, and pKa of five initial LNP formulations. (C) Schematic describing association assay procedure. (D) Association efficiency of initial five LNP formulations. DiO fluorescence readings were used to calculate association efficiency, with association efficiency representing the ratio of fluorescence post-wash to pre-wash with subtraction of background fluorescence for normalization ($n \geq 3$). (E) Percentage of GFP^+ HepG2 cells—measured via flow cytometry—24 h post treatment with initial five LNP formulations ($n = 4$).

tested to evaluate if increased surface modification could alter LNP physiochemical characteristics and cellular interaction. To evaluate this, folate and maleimide LNPs were synthesized in 1:4, 1:3, and 1:1 M ratios (Figure 3A), and the resulting LNPs were characterized as before.

Increasing modifications caused an increase in LNP size, with maleimide particles reaching sizes of 142 nm. Folate-modified LNPs increased in size even more drastically, and at the 1:1 ratio, the presence of folate-PEG caused aggregation of LNPs to greater than 1-μm sizes. Zeta potential, encapsulation efficiency, and pKa had ranges of 5.3–13 mV, 86–94%, and 4.17–5.68, respectively (Figure 3B). Interestingly, increasing modifications seemed to decrease LNP surface charge (Figure S1B). For the folate functionalized LNPs, the zeta potential was lower than the base LNP, while for the maleimide functionalized LNPs the zeta potential was closer to the base LNP. Cytotoxicity remained similar, with all LNPs resulting in cell viability similar to the base LNP control (Figure S1C).

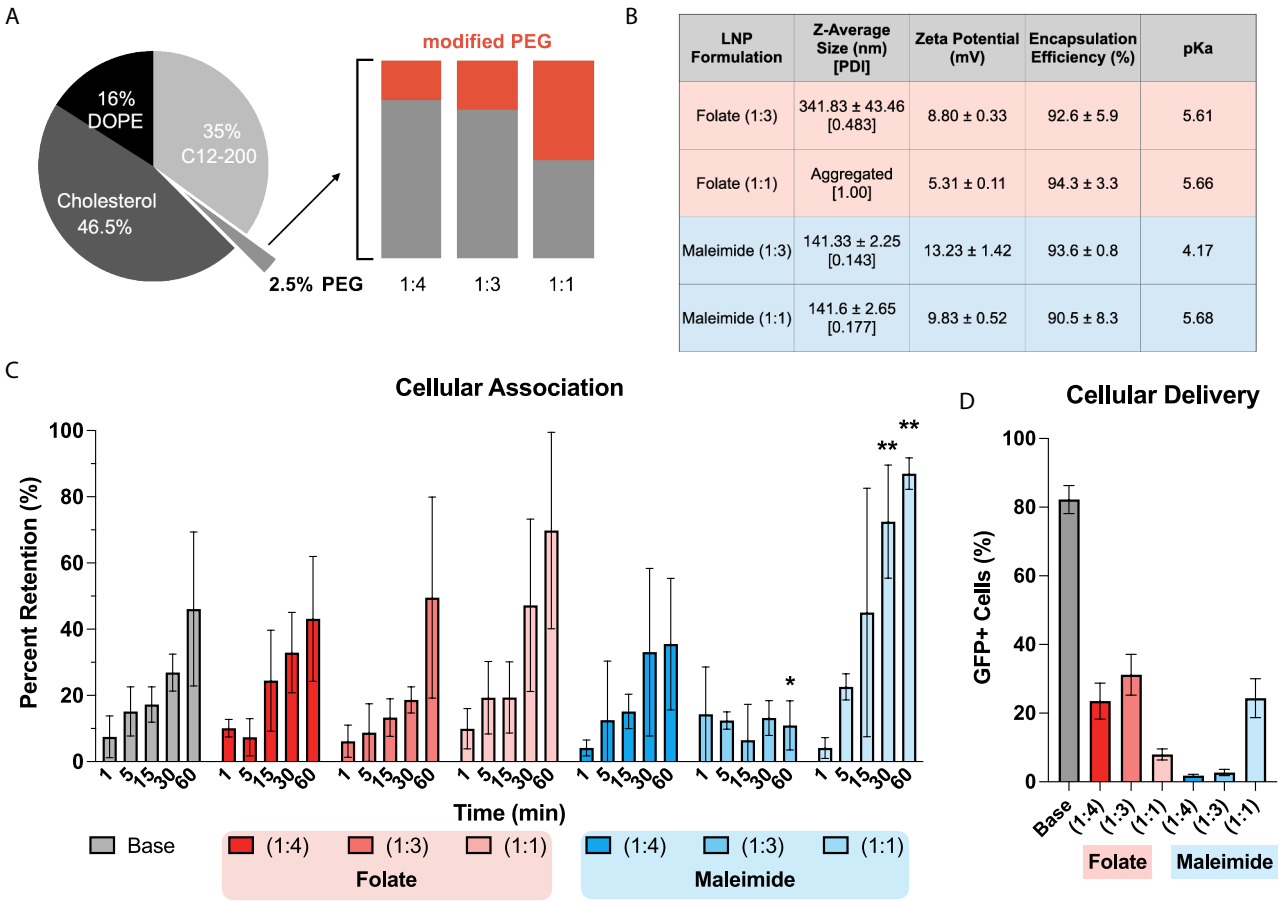

LNP Formulation	Z-Average Size (nm) [PDI]	Zeta Potential (mV)	Encapsulation Efficiency (%)	pKa
Folate (1:3)	341.83 ± 43.46 [0.483]	8.80 ± 0.33	92.6 ± 5.9	5.61
Folate (1:1)	Aggregated [1.00]	5.31 ± 0.11	94.3 ± 3.3	5.66
Maleimide (1:3)	141.33 ± 2.25 [0.143]	13.23 ± 1.42	93.6 ± 0.8	4.17
Maleimide (1:1)	141.6 ± 2.65 [0.177]	9.83 ± 0.52	90.5 ± 8.3	5.68

Figure 3. Transfection and association efficiency of alternative ratios of maleimide and folate functionalized PEG-lipid LNPs

(A) Modification ratios of functionalized PEG-lipid to nonmodified PEG in 2.5% PEG constituent. Maleimide and folate functionalized PEGs were introduced at 1:4, 1:3, and 1:1 ratios. (B) Measurements of z-average, PDI, zeta potential, mRNA encapsulation efficiency, and pKa of maleimide and folate modified LNPs. (C) Association efficiency of base particle and all maleimide and folate functionalized LNPs. DiO fluorescence readings were used to calculate association efficiency, with association efficiency representing the ratio of fluorescence post-wash to pre-wash with subtraction of background fluorescence for normalization (n = 3). ANOVA was used to determine significance between experimental groups and the base LNP at each time point. (D) Percentage of GFP$^+$ HepG2 cells 24 h post treatment (n = 4). *$p < 0.05$; **$p < 0.01$.

Cellular association increased with increased amounts of functionalized PEG-lipids. Both folate (1:1) and maleimide (1:1) functionalized LNPs showed higher maximum values at 30 and 60 min, and in the case of maleimide, this increase was statistically significant when compared with the base LNP. This association assay was additionally tested in a lung cancer cell line (Figure S2), and similar trends were seen: increased association with increased amounts of functionalized PEG. When these LNPs were evaluated for intracellular delivery and expression of mRNA (Figures 3D and S3), all LNPs underperformed in comparison to the base LNP formulation. However, maleimide (1:1) functionalized LNPs resulted in an increase in mRNA delivery, with approximately 20% of cells producing GFP. This potentially hints at a threshold of maleimide content that transitions the interaction of LNPs with the cell surface from association to uptake.

Microscopy for analyzing cellular association and uptake

Due to the generalized measurements of the association assays used previously, it was of interest to evaluate cellular interactions on a more individual basis. While the preliminary association assays assessed potential LNP binding to cancer cells, further visual confirmation was required. To do so, folate and maleimide LNPs, at all three ratios tested, were used to treat HepG2 cells for 1 or 15 min, after which the media and LNPs were removed, and cells were fixed and processed for confocal imaging.

Interestingly, even though the base particle showed significant association and uptake in previous assays, minimal LNP signal was observed. In contrast, all surface modified LNP groups had clear LNP signal at the 15-min time point, and many had substantial signal at the 1-min time point as well (Figure 4A). At the 1-min

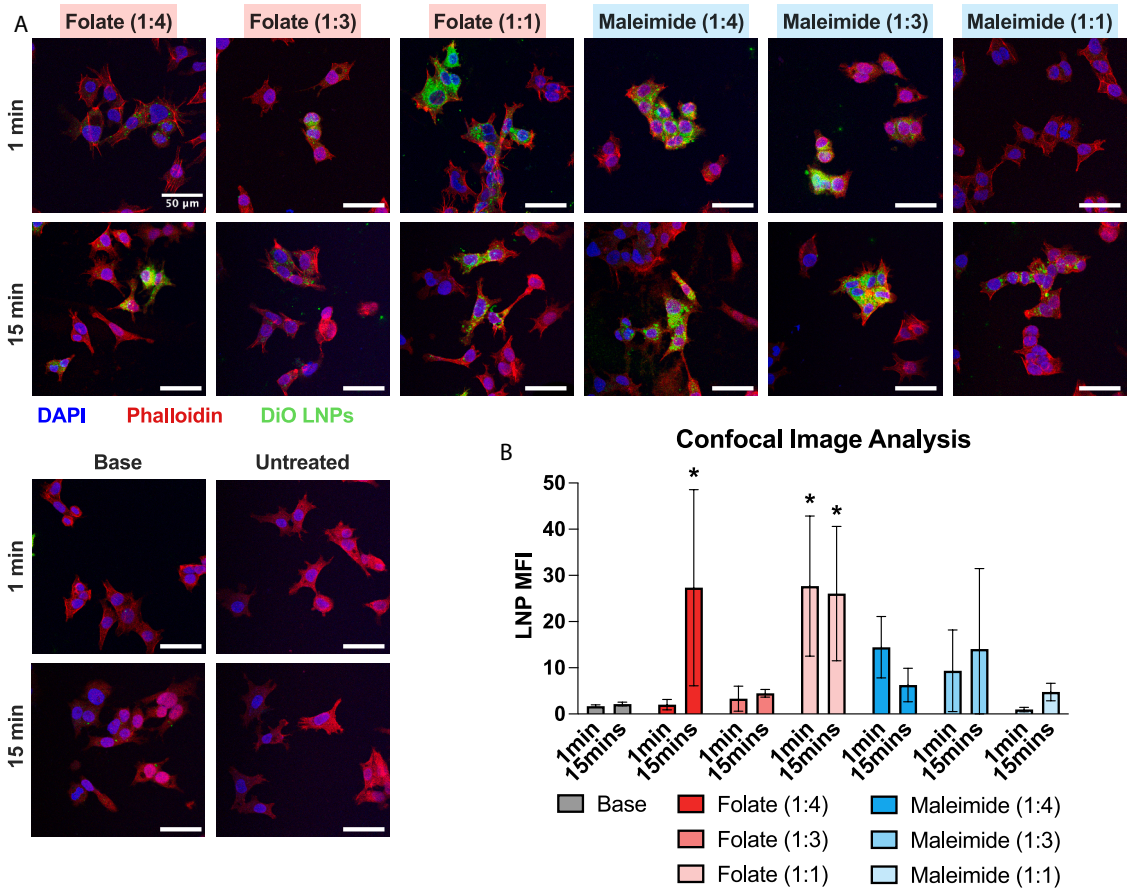

Figure 4. Confocal microscopy analysis of LNP association to HepG2 cells

(A) Representative confocal images at 1 min and 15 min treatment time points. DAPI (blue) shows cell nucleus, phalloidin stain (red) is used to identify cell boundaries, and DiO (green) lipophilic dye indicates LNPs. Scale bar, 50 μm. (B) Mean fluorescence intensity of DiO dye within the cell area, calculated using phalloidin to identify cellular boundaries ($n = 4$). ANOVA was used to determine significance between experimental groups and the base LNP at each time point. *$p < 0.05$.

time point, folate (1:1) LNPs outperformed all other LNPs, based on image analysis and LNP dye intensity (Figure 4B). At the 15-min time point, folate (1:1) and folate (1:4) LNPs were top performers. Of note, in many of the top performing groups, LNP signal was observed in cell clusters, as opposed to individual cells. This may indicate that extracellular interactions between cells play a role in the interaction between surface modified LNPs and cancer cells. In contrast, the base formulation is found minimally in all cells, regardless of clustering.

In vivo intratumoral delivery in a xenograft model of hepatoblastoma

Due to the increased LNP signal at sites of multiple cell clusters, it was of interest to evaluate LNP interaction with tumor cells in an *in vivo* model. GFP^+ HepG2 cells were used to inoculate nude (Nu/J) mice, and after 2 weeks of growth, DiR-dyed LNPs were intratumorally (IT) injected with PBS, base, maleimide (1:4), or folate (1:4) LNPs at a dose of 1 mg/kg mRNA. To assess stability, the size of maleimide (1:4) and folate (1:4) LNPs were tested over time at body temperature (37°C), and neither LNP showed significant size increase (indicating instability) during the times tested (Figure S1D).

The 1-h and 4-h time points post treatment were used for both in vivo imaging system (IVIS) imaging of tumors and confocal imaging of tumor slices. IVIS imaging shows strong presence of LNPs within tumors at both the 1-h and 4-h time points, and while it is not significant (analyzed by ANOVA), there seems to be an increase in signal in the folate (1:4) group, at both time points (Figure 5A), when normalized to tumor size, via GFP fluorescence intensity. Interestingly, the base formulation appeared disperse throughout the entire tumor area, while the folate and maleimide functionalized LNPs were primarily retained near the injection point, where the DiR LNP signal is strongest.

After IVIS imaging, tumors were fixed and processed for imaging. In confocal images of the tumor tissue, there is more clearly identifiable LNP signal in the folate and maleimide functionalized LNPs

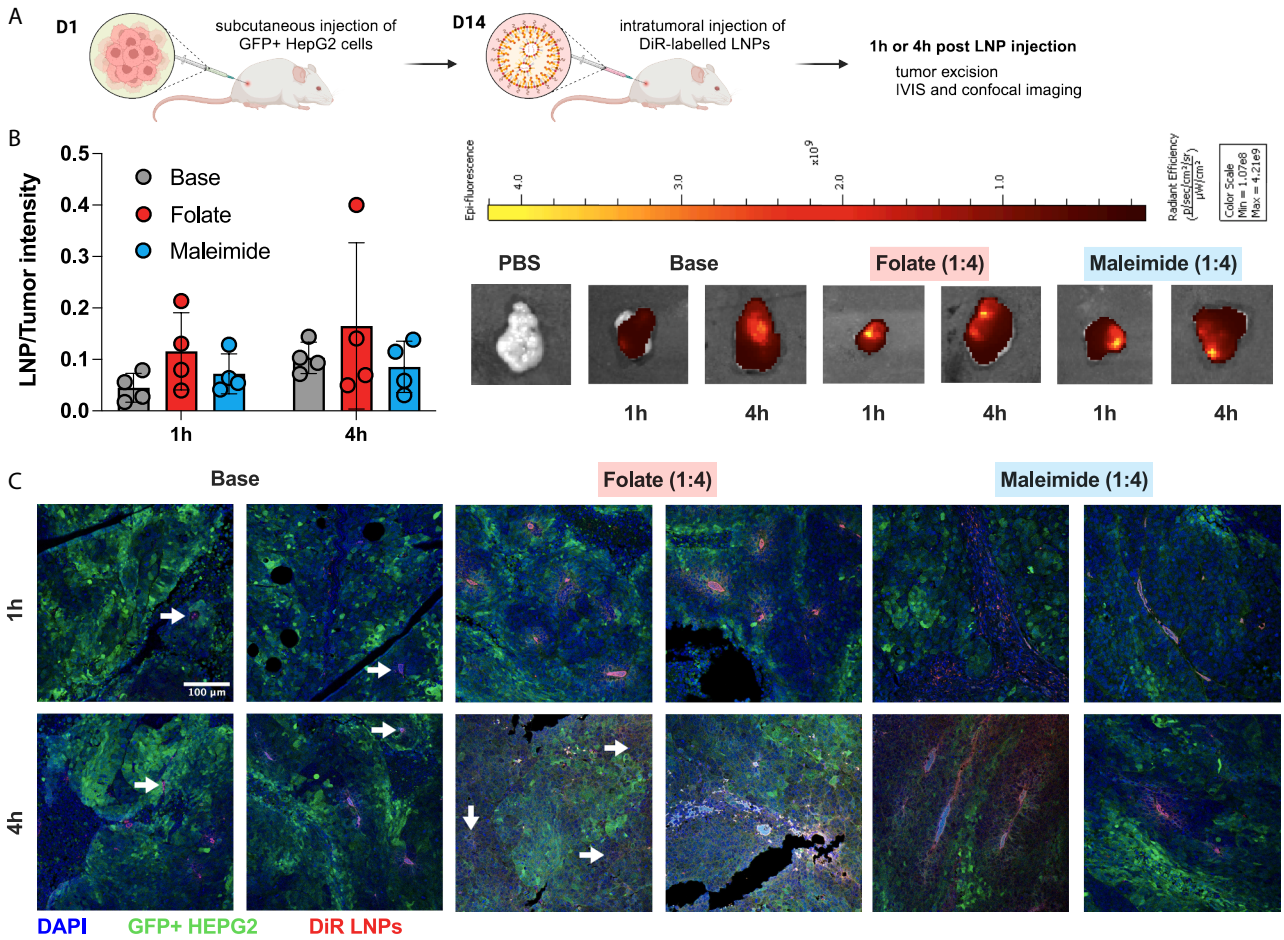

Figure 5. Imaging of xenograft tumors IT injected with base, folate (1:4), or maleimide (1:4) LNPs

(A) Schematic showing timeline of tumor mouse model experiment. (B) Quantification of IVIS images of excised tumors shows a slight increase in DiR signal in the folate group at both time points tested, when signal is normalized to the size of the tumor. In the IVIS images themselves, there are clear injection sites—with strong LNP signal—in the folate and maleimide functionalized LNP groups, while the base formulation seems to be more generally diffuse ($n = 4$). (C) Histology imaging via confocal microscopy of tumor slices 1 h and 4 h post treatment. DAPI (blue) indicates cell nucleus, GFP (green) indicates HepG2 cancer cells, and DiR (red) indicates the presence of LNPs. Scale bar, 100 µm. Areas of DiR signal that may be difficult to visualize are highlighted with white arrows.

groups than the base LNP formulation. At the 4-h time point specifically, there appears to be colocalization of LNP signal in the tumor cells in the folate group.

DISCUSSION

Our study presents advancements in the understanding of using functionalized PEG-lipids within LNP formulations to increase retention of LNP-delivered cancer therapies within the TME. In general, LNPs formulated with different PEG-lipids in some cases retained many of the same physiochemical characteristics but reacted very differently with cells.

According to previous literature, the threshold for small vs. larger LNPs is approximately 100 nm.[47] While the size of the base particle is under this threshold, at 84 nm, all folate-modified LNPs far exceed it, and the higher concentration maleimide LNPs (1:3 and 1:1) slightly exceed it as well, at approximately 140 nm. Larger sized LNPs with PEG-modification have been demonstrated in previous studies,[32,33] and, given that folate has a larger molecular weight than PEG-maleimide, it is plausible that it would have similar—and possibly more exaggerated—effects on the synthesized LNP size. Larger sized particles are generally perceived negatively in the realm of systemically administered drug delivery vehicles. However, recent studies have found that larger molecular size IT administered agents can maximize tumor retention.[48] Therefore, in the context of this study, larger size LNPs could be advantageous. However, in the *in vivo* study, the maleimide (1:4) formulation used is not considered to be a large particle—with a size of 100 nm—and still performs similarly to folate (1:4). Therefore, it is likely that while increased size is affecting tumor retention, it is not the singular cause of the differences seen herein.

Our findings also showed that the amount of functionalized PEG-lipid added to an LNP formulation is a factor for LNP formulation, physicochemical properties, and performance. As the amount of modification increased, particularly for PEG-folate-modified LNPs, the particle size increased substantially. Additionally, increased inclusion of PEG-folate and PEG-maleimide decreased the apparent surface charge of LNPs. This suggests that there may be a threshold beyond which increasing the PEG-conjugate content could negatively impact the physicochemical properties of the LNPs, leading to reduced functionality as a delivery vehicle, regardless of retention properties.

The base formulation shows the greatest transfection efficiency among the LNPs tested, underscoring the efficacy of the previously optimized LNP system. Converse to transfection efficiency, PEG-folate- and PEG-maleimide-modified LNPs showed superior association efficiency *in vitro* and *in vivo*, particularly at shorter time points. The PEG-folate-modified LNPs enhanced association efficiency may be in part attributed to the low dissociation constant (0.1 nmol/L) between folate and folate receptors, which are commonly overexpressed on cancer cells.[30,31,49] Regardless of mechanism, the high association efficiency at low time points *in vitro* is encouraging, as the random vascular nature of the TME can quickly diffuse IT injected agents out into system circulation, and improvements in immediate association with cancer cells may significantly improve delivery.[16]

The *in vivo* assays complemented our *in vitro* assays, providing an analysis of LNP behavior in both controlled environments and within the complex biology of a living organism. *In vivo* IT injected LNPs seemed to stay present in tumors at 1 h and 4 h post injection as IVIS imaging showed DiR signal at both time points across all LNPs. Similarly, confocal images of the same tumor tissue showed LNP presence at the membranes of cancer cells.

Conclusions

Our investigation into the use of functionalized PEG-lipids in LNP formulations holds potential for enhancing the retention of LNPs within the TME. The optimized LNP formulations with PEG-folate and PEG-maleimide modifications have demonstrated superior association to cells of interest, indicating their potential in targeted drug delivery applications. Despite some unexpected findings in terms of transfection efficiency and size-related performance, the overall results underscore the significance of fine-tuning LNP characteristics to maximize therapeutic outcomes.

Future work should aim to elucidate the precise mechanisms governing these results. Advanced characterization techniques, such as cryo-electron microscopy, could provide insights into the nano-architecture of these LNPs, potentially identifying structural anomalies that contribute to the observed biological behaviors. Additionally, exploring the dynamic interactions between LNPs and the TME *in vivo* over extended periods post injection could offer valuable data on the long-term retention and therapeutic efficacy of these formulations. Employing animal models with various tumor types could also determine the versatility and specificity of the PEG-folate and PEG-maleimide modified LNPs. Such studies might validate the broad applicability or indicate a need for further customization.

This study serves as a proof of concept toward the development of more effective LNP-based intratumoral therapeutic delivery systems, highlighting the need for a delicate balance between particle design and biological function. mRNA is an exciting therapeutic modality in oncology as there are multiple proteins that could be therapeutically used in a local delivery platform, including immune-activators such as interleukin-12 and tumor suppressors such as p53, as well as personalized cancer vaccines—which are currently being developed with the rise of precision medicine. Overall, the goal of improving cancer treatment modalities through advanced localized drug delivery systems holds signficant potential.

MATERIALS AND METHODS

Formulation of LNPs

To create the base LNP formulation, mixing of an ethanol phase and aqueous phase was carried out using a staggered herringbone microfluidic mixing device with a 3:1 volume ratio (citrate buffer: ethanol, *v*/*v*) using pump33DS syringe pumps (Harvard Apparatus; Holliston, MA, USA).[50] The ethanol phase contained the ionizable lipid C12-200 with cholesterol (Sigma-Aldrich; St. Louis, MO, USA), DOPE (Avanti Polar Lipids; Alabaster, AL, USA), and 1,2-dimyristoyl-*sn*-glycero-3-phosphoethanolamine-*N*-[methoxy (PEG)-2000 (C14-PEG-2000, PEG, Avanti Polar Lipids) at a 35:46. 5:16:2.5 M ratio in a total volume of 300 μL C12-200 was synthesized by reacting epoxide-terminated alkyl chains (Avanti Polar Lipids) with polyamine cores (Enamine, Monmouth Junction, NJ, USA) using nucleophilic addition/SN2 reactions, as previously described.[51] The aqueous phase contained 10 mM citrate buffer and either mCherry or GFP mRNA at weight ratio of 10:1 (ionizable lipid:mRNA), in a total volume of 900 μL, kindly gifted from the Weissman Lab at the University of Pennsylvania (Philadelphia, PA, USA).

For experimental LNP formulations, 1,2-distearoyl-sn-glycero-3-phosphoethanolamine-N-[carboxy(PEG)-2000] (DSPE-PEG(2000) carboxylic acid), 1,2-distearoyl-sn-glycero-3-phosphoethanolamine-N-[folate(PEG)-2000] (DSPE-PEG(2000) folate), 1,2-distearoyl-sn-glycero-3-phosphoethanolamine-N-[3-(2-pyridyldithio) propionate (PEG)-2000] (DSPE-PEG(2000) PDP), or 1,2-distearoyl-sn-glycero-3-phosphoethanolamine-N-[maleimide(PEG)-2000] (DSPE-PEG(2000) maleimide) were purchased from Avanti Polar Lipids and substituted for a percentage of the 2.5 M ratio of PEG, at a molar ratio of 1:4, 1:3 and 1:1 (functionalized-PEG:non-modified PEG).

The resulting LNP solution was dialyzed against 1× PBS in 20-kDa molecular weight cutoff dialysis cassettes for 2 h and subsequently

sterilely filtered via 0.44 μm syringe filters (Genesee Scientific, El Cajon, CA, USA). Final LNP solution was stored at 4°C until use.

LNP characterization

For dynamic light scattering measurements, LNPs were diluted at a 1:99 ratio with 1× PBS at 1 mL total volume in 4-mL disposable cuvettes. The Zetasizer Nano (Malvern Instruments, Malvern, UK) was used to determine LNP size (Z-average diameter) and PDI of all LNPs, reported with mean ± SD (n = 3 measurements).

For zeta potential measurements, LNPs were diluted at a 1:49 ratio in molecular biology water and resulting solution was put in DTA1070 zeta potential cuvettes (Malvern Panalytical, Malvern, UK). Zetasizer Nano instrument was used and reported LNP surface zeta potential as mean ± SD (n = 3 measurements).

mRNA encapsulation efficiency was determined using the Quant-iT RiboGreen RNA Assay Kit (Thermo Fisher Scientific, Waltham, MA, USA) as described by manufacturer's protocol. LNPs were diluted 100× in either 1× TE buffer or 0.1% Triton X-100 in 1× TE buffer (Sigma Aldrich), and encapsulation efficiency was determined by comparing the mRNA concentration of unencapsulated mRNA (TE buffer samples) to encapsulated mRNA (Triton X-100 samples). Data are reported as the mean ± SD (n = 3 measurements).

To determine LNP pKa, a 6-(ptoluidinyl)naphthalene-2-sulfonic acid (TNS) assay was used to measure surface ionization as previously described.[51] Buffered solutions of 150 mM sodium chloride, 20 mM sodium phosphate, 25 mM ammonium citrate, and 20 mM ammonium acetate were adjusted to reach pH values ranging from 2 to 12 in increments of 0.5. LNPs were added to each pH-adjusted solution in triplicate wells in a 96-well plate. TNS was then added to each well to reach a final concentration of 6 μM, The resulting fluorescence was measured on the Infinite M Plex plate reader. The resulting data were fit with a sigmoidal regression, and the pK_a was calculated as the pH at which the fluorescence intensity reached 50% of its maximum value. Data are reported as the mean ± SD (n = 3 measurements).

Cell culture

For all *in vitro* studies, HepG2 cells were cultured in DMEM supplemented with 10% fetal bovine serum and 1% penicillin-streptomycin. Cells were stored in an incubator at 37°C with standard humidity and CO_2 levels and were passaged once reaching 70% confluence.

Flow cytometry analysis

HepG2 cells were plated in a 96-well plate at 10,000 cells per well in 60 μL of DMEM. After 24 h, cells were treated with LNPs encapsulating GFP mRNA at a dosage of 100 ng mRNA per well. At 24 h post treatment, cells were washed once with cold 1× PBS, detached with 0.25% trypsin, and pelleted in a 4°C tabletop centrifuge at 300 rcf. Cell pellets were resuspended in 1× PBS with 0.5 μL of SYTOX Red Live/Dead stain (Thermo Fisher Scientific), and samples were analyzed on the BD LSR II Flow Cytometer (BD Biosciences, Franklin Lakes, NJ, USA). At least 10,000 total events were collected. Data were analyzed with FlowJo v10 (BD Biosciences) and reported as the mean ± SD (n = 3 measurements).

Dyeing of mRNA LNPs

To track LNPs *in vitro* and *in vivo*, mRNA LNPs were stained via addition of 1 μL of 1 mM Vybrant DiO or DiR Cell-Labeling Solution (Thermo Fisher Scientific) per 100 μL of LNP solution. LNPs were subsequently shaken for 30 min at 37°C. To remove excess dye, dyed LNPs were filtered using a 10kDa Amicon Ultra Centrifugal Filter (Millipore Sigma) via centrifuge at 800×g for 30 min.

mRNA LNP association assay

HepG2 cells used for the mRNA LNP association assay were cultured in clear DMEM (Thermo Fisher Scientific) to avoid background fluorescence in eventual readout. Cells were plated in a 96-well plate at 100,000 cells in 100 μL per well and incubated for 24 h. In this assay, cells are treated at five time points before readout: 60 min, 30 min, 15 min, 5 min, and 1 min. At each time point, cells are treated with 100 ng of mRNA encapsulated within DiO-dyed mRNA LNPs. Between each treatment, the 96-well plate was stored in the incubator to simulate the bodily environment. At 1 min post last treatment (60 min post first treatment), fluorescence measurements for each well were measured using the Infinite M Plex plate reader with excitation = 483 nm and emission = 501 nm. Post initial readout, each well had media removed and was washed with PBS once before addition of 100 μL of 1× PBS for final readout in the plate reader at the same excitation-emission spectra. Both readouts were normalized for background fluorescence and the following equation was used to determine the percent adherence of LNPs to HepG2 membranes for each LNP formulation at each time point.

$$\frac{Flourescence_{final}}{Flourescence_{initial}} = Percent\ of\ LNPs\ adhered\ to\ HepG2\ membranes$$

Confocal microscopy

Well Chamber, Removable (Ibidi) confocal microscopy chamber slides were used for this analysis. Wells were treated with 1 mL of gelatin—to improve cellular adhesion to the imaging surface—and slides were stored overnight in cell culture. Gelatin was then aspirated off and wells were subsequently exposed to UV light for 45 min in a biosafety cabinet. We plated 30,000 HepG2 cells in 300 μL of DMEM media in each well and stored them overnight in cell culture to allow for cell adherence to well bottom. LNPs were dyed with DiO in correspondence to the procedure outlined above before treatment of HepG2 cells. Cells were treated with 100 ng of mRNA encapsulated within LNPs at a 1 min and 15 min time point before cell fixing. This reduced total mRNA dose results in an equivalent mRNA/cell dose, due to the smaller size of the chamber slides 1 min or 15 min post LNP treatment, depending on the time point in

question, media was aspirated, cells were washed once with 1× PBS, and then 300 μL of 4% paraformaldehyde was added to each well and the confocal slide was put in cell culture for 15 min to allow for cell fixing. Cells were subsequently rinsed with PBS three times for 5 min each. We added 300 μL of 5% DyLight 650 Phalloidin in 1× PBS and the confocal slide was allowed to incubate for 15 min to stain the HepG2 cell membrane. Wells were rinsed once with PBS and allowed to dry. Well plastic was then removed and a coverslip with two to three drops of ProLong Gold Antifade Mountant with DAPI was added. Slides were stored in fridge until analysis via confocal microscopy (Zeiss LSM 710; Carl Zeiss Meditec, Jena, Germany). Resulting confocal microscopy images were analyzed using ImageJ software, utilizing the Phalloidin stain to identify cell boundaries and then calculating DiO signal intensity within.

In vivo xenograft model for LNP retention

All animal use was in accordance with the guidelines and approval from the University of Pennsylvania Institution of Animal Care and Use Committee. GFP^+ HepG2 cells (3×10^6) were resuspended in 1× PBS and injected subcutaneously into the flanks of female nude (Nu/J) mice at approximately 8 weeks of age. Two weeks after inoculation, when tumors were visible under the skin and at least 100 mm^3 in volume, IT injections of control 1× PBS and experimental LNPs were carried out. Bioluminescence imaging was performed using an IVIS Spectrum Imaging spectrum (Caliper Life Sciences, Waltham, MA, USA).

Post IVIS imaging, tumors were collected and fixed in 10% neutral buffered formalin for at least 24 h. Fixed tissue was processed and embedded by the histotechnology facility at the Wistar Institute, to produce DAPI-stained tissue slides. Images were collected using confocal microscopy (Zeiss LSM 710), where the nucleus of cells is identified *via* DAPI stain (blue), tumor cells are identified *via* expression of GFP (green), and LNP presence is identified *via* DiR stain (red).

Statistical analysis

Statistical analyses were performed on GraphPad Prism (v10) software. If otherwise unspecified, ANOVA was applied as appropriate. Statistical significance was defined at $\alpha = 0.05$. Multiple batches of LNP and mRNA were used throughout this study.

DATA AVAILABILITY

Additional data are available in the supplementary file for this manuscript or on request from the authors.

ACKNOWLEDGMENTS

R.M.H. was supported by the National Science Foundation Graduate Research Fellowship Program (NSF-GRFP) under Grant No. DGE-2236662. M.M.B. was supported by a U.S. National Institutes of Health (NIH) Ruth L. Kirschstein National Research Service Award (F31 CA260922). M.J.M. was supported by a NIH Director's New Innovator Award (DP2 TR002776), a Burroughs Wellcome Fund Career Award at the Scientific Interface (CASI), an American Cancer Society Research Scholar Grant (RSG-22-122-01-ET), and an NSF CAREER Award (CBET-2145491).

Data for this manuscript were generated using the Penn Cytomics and Cell Sorting Shared Resource Laboratory at the University of Pennsylvania and are partially supported by the Abramson Cancer Center NCI Grant (P30 016520, RRid:SCR 022376). Images were collected using instruments at the Cell & Developmental Biology (CDB) Microscopy Core, in the Perelman School of Medicine at the University of Pennsylvania. We are also grateful to the Wistar Institute's Histotechnology Facility for providing technical support. Funding support for The Wistar Institute core facilities was provided by Cancer Center Support Grant P30 CA010815.

AUTHOR CONTRIBUTIONS

M.J., R.M.H., and M.M.B. were responsible for initial project conceptualization and planning. M.J. and R.M.H were responsible for data collection, analysis, and preparing the original manuscript draft. C.F.E and X.H. aided in data collection and analysis. M.J. M. acquired funding and resources needed for this work. All authors reviewed and edited the final manuscript.

DECLARATION OF INTERESTS

The authors declare no competing interests.

SUPPLEMENTAL INFORMATION

Supplemental information can be found online at https://doi.org/10.1016/j.omtm.2025.101457.

REFERENCES

1. Siegel, R.L., Giaquinto, A.N., and Jemal, A. (2024). Cancer statistics, 2024. CA Cancer J. Clin. *74*, 12–49. https://doi.org/10.3322/caac.21820.
2. Paresishvili, T., and Kakabadze, Z. (2023). Challenges and Opportunities Associated With Drug Delivery for the Treatment of Solid Tumors. Oncol. Rev. *17*, 10577. https://doi.org/10.3389/or.2023.10577.
3. Chua, C.Y.X., Ho, J., Demaria, S., Ferrari, M., and Grattoni, A. (2020). Emerging Technologies for Local Cancer Treatment. Adv. Ther. *3*, 2000027. https://doi.org/10.1002/adtp.202000027.
4. Butowska, K., Han, X., Gong, N., El-Mayta, R., Haley, R.M., Xue, L., Zhong, W., Guo, W., Wang, K., and Mitchell, M.J. (2023). Doxorubicin-conjugated siRNA lipid nanoparticles for combination cancer therapy. Acta Pharm. Sin. B *13*, 1429–1437. https://doi.org/10.1016/j.apsb.2022.07.011.
5. Wilhelm, S., Tavares, A.J., Dai, Q., Ohta, S., Audet, J., Dvorak, H.F., and Chan, W.C. W. (2016). Analysis of nanoparticle delivery to tumours. Nat. Rev. Mater. *1*, 16014. https://doi.org/10.1038/natrevmats.2016.14.
6. Mitchell, M.J., Billingsley, M.M., Haley, R.M., Wechsler, M.E., Peppas, N.A., and Langer, R. (2021). Engineering precision nanoparticles for drug delivery. Nat. Rev. Drug Discov. *20*, 101–124. https://doi.org/10.1038/s41573-020-0090-8.
7. Sindhwani, S., Syed, A.M., Ngai, J., Kingston, B.R., Maiorino, L., Rothschild, J., MacMillan, P., Zhang, Y., Rajesh, N.U., Hoang, T., et al. (2020). The entry of nanoparticles into solid tumours. Nat. Mater. *19*, 566–575. https://doi.org/10.1038/s41563-019-0566-2.
8. Subhan, M.A., Yalamarty, S.S.K., Filipczak, N., Parveen, F., and Torchilin, V.P. (2021). Recent Advances in Tumor Targeting via EPR Effect for Cancer Treatment. J. Pers. Med. *11*, 571. https://doi.org/10.3390/jpm11060571.
9. Sheth, R.A., Wehrenberg-Klee, E., Patel, S.P., Brock, K.K., Fotiadis, N., and de Baère, T. (2024). Intratumoral Injection of Immunotherapeutics: State of the Art and Future Directions. Radiology *312*, e232654. https://doi.org/10.1148/radiol.232654.
10. Zhou, Y., Chen, X., Cao, J., and Gao, H. (2020). Overcoming the biological barriers in the tumor microenvironment for improving drug delivery and efficacy. J. Mater. Chem. B *8*, 6765–6781. https://doi.org/10.1039/D0TB00649A.
11. Chauhan, V.P., Stylianopoulos, T., Boucher, Y., and Jain, R.K. (2011). Delivery of Molecular and Nanoscale Medicine to Tumors: Transport Barriers and Strategies. Annu. Rev. Chem. Biomol. Eng. *2*, 281–298. https://doi.org/10.1146/annurev-chembioeng-061010-114300.
12. Krammer, F., Srivastava, K., Alshammary, H., Amoako, A.A., Awawda, M.H., Beach, K.F., Bermúdez-González, M.C., Bielak, D.A., Carreño, J.M., Chernet, R.L., et al. (2021). Antibody Responses in Seropositive Persons after a Single Dose of

SARS-CoV-2 mRNA Vaccine. N. Engl. J. Med. *384*, 1372–1374. https://doi.org/10.1056/NEJMc2101667.

13. Zhang, L., More, K.R., Ojha, A., Jackson, C.B., Quinlan, B.D., Li, H., He, W., Farzan, M., Pardi, N., and Choe, H. (2023). Effect of mRNA-LNP components of two globally-marketed COVID-19 vaccines on efficacy and stability. NPJ Vaccines *8*, 156. https://doi.org/10.1038/s41541-023-00751-6.

14. Vogel, A.B., Kanevsky, I., Che, Y., Swanson, K.A., Muik, A., Vormehr, M., Kranz, L. M., Walzer, K.C., Hein, S., Güler, A., et al. (2021). BNT162b vaccines protect rhesus macaques from SARS-CoV-2. Nature *592*, 283–289. https://doi.org/10.1038/s41586-021-03275-y.

15. Akanda, M., Mithu, M.S.H., and Douroumis, D. (2023). Solid lipid nanoparticles: An effective lipid-based technology for cancer treatment. J. Drug Deliv. Sci. Technol. *86*, 104709. https://doi.org/10.1016/j.jddst.2023.104709.

16. Miller, A.D. (2013). Lipid-Based Nanoparticles in Cancer Diagnosis and Therapy. J. Drug Deliv. *2013*, 165981. https://doi.org/10.1155/2013/165981.

17. Li, Y., Ye, Z., Yang, H., and Xu, Q. (2022). Tailoring combinatorial lipid nanoparticles for intracellular delivery of nucleic acids, proteins, and drugs. Acta Pharm. Sin. B *12*, 2624–2639. https://doi.org/10.1016/j.apsb.2022.04.013.

18. Haley, R.M., Chan, A., Billingsley, M.M., Gong, N., Padilla, M.S., Kim, E.H., Wang, H., Yin, D., Wangensteen, K.J., Tsourkas, A., and Mitchell, M.J. (2023). Lipid Nanoparticle Delivery of Small Proteins for Potent *In Vivo* RAS Inhibition. ACS Appl. Mater. Interfaces *15*, 21877–21892. https://doi.org/10.1021/acsami.3c01501.

19. Chen, S., Huang, X., Xue, Y., Álvarez-Benedicto, E., Shi, Y., Chen, W., Koo, S., Siegwart, D.J., Dong, Y., and Tao, W. (2023). Nanotechnology-based mRNA vaccines. Nat. Rev. Methods Primers *3*, 63. https://doi.org/10.1038/s43586-023-00246-7.

20. Zhang, Z., Yao, S., Hu, Y., Zhao, X., and Lee, R.J. (2022). Application of lipid-based nanoparticles in cancer immunotherapy. Front. Immunol. *13*, 967505. https://doi.org/10.3389/fimmu.2022.967505.

21. Xu, X., and Xia, T. (2023). Recent Advances in Site-Specific Lipid Nanoparticles for mRNA Delivery. ACS Nanosci. Au *3*, 192–203. https://doi.org/10.1021/acsnanoscienceau.2c00062.

22. Marques, A.C., Costa, P.C., Velho, S., and Amaral, M.H. (2023). Lipid Nanoparticles Functionalized with Antibodies for Anticancer Drug Therapy. Pharmaceutics *15*, 216. https://doi.org/10.3390/pharmaceutics15010216.

23. Lee, D.Y., Amirthalingam, S., Lee, C., Rajendran, A.K., Ahn, Y.-H., and Hwang, N.S. (2023). Strategies for targeted gene delivery using lipid nanoparticles and cell-derived nanovesicles. Nanoscale Adv. *5*, 3834–3856. https://doi.org/10.1039/D3NA00198A.

24. Mishra, P., Nayak, B., and Dey, R.K. (2016). PEGylation in anti-cancer therapy: An overview. Asian J. Pharm. Sci. *11*, 337–348. https://doi.org/10.1016/j.ajps.2015.08.011.

25. Huang, X., Kong, N., Zhang, X., Cao, Y., Langer, R., and Tao, W. (2022). The landscape of mRNA nanomedicine. Nat. Med. *28*, 2273–2287. https://doi.org/10.1038/s41591-022-02061-1.

26. Caliceti, P., and Veronese, F.M. (2003). Pharmacokinetic and biodistribution properties of poly(ethylene glycol)–protein conjugates. Adv. Drug Deliv. Rev. *55*, 1261–1277. https://doi.org/10.1016/S0169-409X(03)00108-X.

27. Blanco, E., Shen, H., and Ferrari, M. (2015). Principles of nanoparticle design for overcoming biological barriers to drug delivery. Nat. Biotechnol. *33*, 941–951. https://doi.org/10.1038/nbt.3330.

28. Knop, K., Hoogenboom, R., Fischer, D., and Schubert, U.S. (2010). Poly(ethylene glycol) in Drug Delivery: Pros and Cons as Well as Potential Alternatives. Angew. Chem. Int. Ed. Engl. *49*, 6288–6308. https://doi.org/10.1002/anie.200902672.

29. Young, O., Ngo, N., Lin, L., Stanbery, L., Creeden, J.F., Hamouda, D., and Nemunaitis, J. (2023). Folate Receptor as a Biomarker and Therapeutic Target in Solid Tumors. Curr. Probl. Cancer *47*, 100917. https://doi.org/10.1016/j.currprobl-cancer.2022.100917.

30. Frigerio, B., Bizzoni, C., Jansen, G., Leamon, C.P., Peters, G.J., Low, P.S., Matherly, L. H., and Figini, M. (2019). Folate receptors and transporters: biological role and diagnostic/therapeutic targets in cancer and other diseases. J. Exp. Clin. Cancer Res. *38*, 125. https://doi.org/10.1186/s13046-019-1123-1.

31. Ye, W.l., Du, J.b., Zhang, B.l., Na, R., Song, Y.f., Mei, Q.b., Zhao, M.g., and Zhou, S.y. (2014). Cellular Uptake and Antitumor Activity of DOX-hyd-PEG-FA Nanoparticles. PLoS One *9*, e97358. https://doi.org/10.1371/journal.pone.0097358.

32. Billingsley, M.M., Gong, N., Mukalel, A.J., Thatte, A.S., El-Mayta, R., Patel, S.K., Metzloff, A.E., Swingle, K.L., Han, X., Xue, L., et al. (2024). In Vivo mRNA CAR T Cell Engineering via Targeted Ionizable Lipid Nanoparticles with Extrahepatic Tropism. Small *20*, e2304378. https://doi.org/10.1002/smll.202304378.

33. Metzloff, A.E., Padilla, M.S., Gong, N., Billingsley, M.M., Han, X., Merolle, M., Mai, D., Figueroa-Espada, C.G., Thatte, A.S., Haley, R.M., et al. (2024). Antigen Presenting Cell Mimetic Lipid Nanoparticles for Rapid mRNA CAR T Cell Cancer Immunotherapy. Adv. Mater. *36*, e2313226. https://doi.org/10.1002/adma.202313226.

34. Shtenberg, Y., Goldfeder, M., Schroeder, A., and Bianco-Peled, H. (2017). Alginate modified with maleimide-terminated PEG as drug carriers with enhanced mucoadhesion. Carbohydr. Polym. *175*, 337–346. https://doi.org/10.1016/j.carbpol.2017.07.076.

35. Wang, X., Meng, X., Mao, K., Chen, H., Cong, X., Liu, F., Wang, J., Liu, S., Xin, Y., Zhu, G., et al. (2023). Maleimide as the PEG end-group promotes macrophage-targeted drug delivery of PEGylated nanoparticles in vivo by enhancing interaction with circulating erythrocytes. Biomaterials *300*, 122187. https://doi.org/10.1016/j.biomaterials.2023.122187.

36. Goerdeler, F., Reuber, E.E., Lühle, J., Leichnitz, S., Freitag, A., Nedielkov, R., Groza, R., Ewers, H., Möller, H.M., Seeberger, P.H., and Moscovitz, O. (2023). Thiol-Mediated Uptake of a Cysteine-Containing Nanobody for Anticancer Drug Delivery. ACS Cent. Sci. *9*, 1111–1118. https://doi.org/10.1021/acscentsci.3c00177.

37. Sahaf, B., Heydari, K., Herzenberg, L.A., and Herzenberg, L.A. (2003). Lymphocyte surface thiol levels. Proc. Natl. Acad. Sci. USA *100*, 4001–4005. https://doi.org/10.1073/pnas.2628032100.

38. Schaaf, M.B., Garg, A.D., and Agostinis, P. (2018). Defining the role of the tumor vasculature in antitumor immunity and immunotherapy. Cell Death Dis. *9*, 115. https://doi.org/10.1038/s41419-017-0061-0.

39. Oswald, M., Geissler, S., and Goepferich, A. (2016). Determination of the activity of maleimide-functionalized phospholipids during preparation of liposomes. Int. J. Pharm. *514*, 93–102. https://doi.org/10.1016/j.ijpharm.2016.06.116.

40. Meyer, M., Dohmen, C., Philipp, A., Kiener, D., Maiwald, G., Scheu, C., Ogris, M., and Wagner, E. (2009). Synthesis and Biological Evaluation of a Bioresponsive and Endosomolytic siRNA—Polymer Conjugate. Mol. Pharm. *6*, 752–762. https://doi.org/10.1021/mp9000124.

41. Schmidt, S., Wang, H., Pussak, D., Mosca, S., and Hartmann, L. (2015). Probing multivalency in ligand–receptor-mediated adhesion of soft, biomimetic interfaces. Beilstein J. Org. Chem. *11*, 720–729. https://doi.org/10.3762/bjoc.11.82.

42. Singh, A., Bezuidenhout, M., Walsh, N., Beirne, J., Felletti, R., Wang, S., Fitzgerald, K.T., Gallagher, W.M., Kiely, P., and Redmond, G. (2016). Functionalization of emissive conjugated polymer nanoparticles by coprecipitation: consequences for particle photophysics and colloidal properties. Nanotechnology *27*, 305603. https://doi.org/10.1088/0957-4484/27/30/305603.

43. Anderson, C.R., Hu, X., Zhang, H., Tlaxca, J., Declèves, A.-E., Houghtaling, R., Sharma, K., Lawrence, M., Ferrara, K.W., and Rychak, J.J. (2011). Ultrasound Molecular Imaging of Tumor Angiogenesis With an Integrin Targeted Microbubble Contrast Agent. Investig. Radiol. *46*, 215–224. https://doi.org/10.1097/RLI.0b013e3182034fed.

44. Kauffman, K.J., Dorkin, J.R., Yang, J.H., Heartlein, M.W., DeRosa, F., Mir, F.F., Fenton, O.S., and Anderson, D.G. (2015). Optimization of Lipid Nanoparticle Formulations for mRNA Delivery in Vivo with Fractional Factorial and Definitive Screening Designs. Nano Lett. *15*, 7300–7306. https://doi.org/10.1021/acs.nanolett.5b02497.

45. Cheng, Q., Wei, T., Jia, Y., Farbiak, L., Zhou, K., Zhang, S., Wei, Y., Zhu, H., and Siegwart, D.J. (2018). Dendrimer-Based Lipid Nanoparticles Deliver Therapeutic

FAH mRNA to Normalize Liver Function and Extend Survival in a Mouse Model of Hepatorenal Tyrosinemia Type I. Adv. Mater. *30*, e1805308. https://doi.org/10.1002/adma.201805308.

46. Ball, R.L., Hajj, K.A., Vizelman, J., Bajaj, P., and Whitehead, K.A. (2018). Lipid Nanoparticle Formulations for Enhanced Co-delivery of siRNA and mRNA. Nano Lett. *18*, 3814–3822. https://doi.org/10.1021/acs.nanolett.8b01101.

47. Dammes, N., Goldsmith, M., Ramishetti, S., Dearling, J.L.J., Veiga, N., Packard, A.B., and Peer, D. (2021). Conformation-sensitive targeting of lipid nanoparticles for RNA therapeutics. Nat. Nanotechnol. *16*, 1030–1038. https://doi.org/10.1038/s41565-021-00928-x.

48. Saadat, M., Zahednezhad, F., Zakeri-Milani, P., Reza Heidari, H., Shahbazi-Mojarrad, J., and Valizadeh, H. (2019). Drug Targeting Strategies Based on Charge Dependent Uptake of Nanoparticles into Cancer Cells. J. Pharm. Pharm. Sci. *22*, 191–220. https://doi.org/10.18433/jpps30318.

49. Martínez-Jothar, L., Doulkeridou, S., Schiffelers, R.M., Sastre Torano, J., Oliveira, S., van Nostrum, C.F., and Hennink, W.E. (2018). Insights into maleimide-thiol conjugation chemistry: Conditions for efficient surface functionalization of nanoparticles for receptor targeting. J. Contr. Release *282*, 101–109. https://doi.org/10.1016/j.jconrel.2018.03.002.

50. Shepherd, S.J., Warzecha, C.C., Yadavali, S., El-Mayta, R., Alameh, M.-G., Wang, L., Weissman, D., Wilson, J.M., Issadore, D., and Mitchell, M.J. (2021). Scalable mRNA and siRNA Lipid Nanoparticle Production Using a Parallelized Microfluidic Device. Nano Lett. *21*, 5671–5680. https://doi.org/10.1021/acs.nanolett.1c01353.

51. Billingsley, M.M., Singh, N., Ravikumar, P., Zhang, R., June, C.H., and Mitchell, M.J. (2020). Ionizable Lipid Nanoparticle-Mediated mRNA Delivery for Human CAR T Cell Engineering. Nano Lett. *20*, 1578–1589. https://doi.org/10.1021/acs.nanolett.9b04246.